PID and State Feedback Controllers Using DNA Strand Displacement Reactions

Nuno M. G. Paulino, Mathias Foo, Jongmin Kim, and Declan G. Bates

***Abstract*—Nucleic acid-based chemistry is a strong candidate framework for the construction of future synthetic biomolecular control circuits. Previous work has demonstrated the capacity of circuits based on DNA strand displacement (DSD) reactions to implement digital and analogue signal processing *in vivo*, including in mammalian cells. To date, however, feedback control system designs attempted within this framework have been restricted to extremely simple proportional or proportional-integral controller architectures. In this letter, we significantly extend the potential complexity of such controllers by showing how time-delays, numerical differentiation (to allow PID control), and state feedback may be implemented via chemical reaction network-based designs. Our controllers are implemented and tested using VisualDSD, a rapid-prototyping tool that allows precise analysis of computational devices implemented using nucleic acids, via both deterministic and stochastic simulations of the DSD reactions.**

***Index Terms*—Biomolecular systems, PID control, control applications.**

I. Introduction

THE CAPABILITY of DNA strand displacement reactions (DSD) to operate *in vivo* and interface with endogenous cellular machinery has been demonstrated in mammalian cells, with engineered oligonucleotide AND gates responding to microRNA inputs [1], multi-input logic based on DNA circuitry interacting with native mRNA [2], and reliable strand displacement probes triggered by mRNA being transcribed into cells [3]. This makes circuits based on nucleic acids strong potential candidates for many computing and control applications in synthetic biology. The frameworks based on DSD reactions [4] use the sequences of the DNA strands to effectively program biochemical circuitry to compute digital and analogue functions [5], [6].

For the purposes of circuit design, chemical reaction networks (CRNs) provide a powerful abstract layer with which to conceptualise biomolecular computations and operations [7], [8], [9], since simple chemical reactions like catalysis, degradation and annihilation can be readily mapped into equivalent DSD reactions [4]. Linear feedback control concepts can then be translated to biomolecular applications through the representation of linear operators using CRNs [7]. Simple proportional and proportional-integral controllers have been designed in [10], [11], [12], where the so-called *dual rail* representation [10] overcomes the limitation of positivity of CRNs, to allow the representation of both positive and negative signals (crucial for the generation of error signals in feedback control) using molecular concentrations. It has also been shown in [13] that any proper transfer function can also be represented with dual rail CRN circuits, hence allowing frequency domain controller designs to be implemented with equivalent DSD reactions, without resorting to linearisation techniques (as in [14]). First steps towards the construction of nonlinear controllers, using sliding mode control architectures, designed using CRN circuits were recently reported in [15]. Sophisticated software toolboxes are also now available that can provide a highly automated translation of CRN-based designs to DNA strands, and simulate the resulting DSD network [16].

Three fundamental limitations of recent efforts to develop a comprehensive theory of feedback control for nucleic acids have been the lack of (a) methods for computing the derivative of a signal (necessary for the implementation of PID controllers), (b) a convenient way to represent time delays, and (c) the ability to implement state feedback controller architectures. Here we propose designs based on CRNs that address each of these open questions, and verify the correct functioning of the resulting PID and state feedback controllers via deterministic and stochastic simulations of the DNA strand displacement network using the VisualDSD rapid prototyping tool [11], [16].

II. Representation of Linear Systems With CRNs

We define a CRN as a set of reactions between chemical species. A reaction between species X_1 and X_2 is

Manuscript received March 1, 2019; revised April 30, 2019; accepted May 18, 2019. Date of publication May 24, 2019; date of current version June 6, 2019. This work was supported in part by Biotechnology and Biological Sciences Research Council (BBSRC)/Engineering and Physical Sciences Research Council (EPSRC) under Grant BB/M017982/1, and in part by EPSRC and BBSRC Centre for Doctoral Training in Synthetic Biology under Grant EP/L016494/1. Recommended by Senior Editor M. Arcak. *(Corresponding author: Nuno M. G. Paulino.)*

N. M. G. Paulino and D. G. Bates are with the Warwick Integrative Synthetic Biology Centre, School of Engineering, University of Warwick, CV4 7AL Coventry, U.K. (e-mail: n.paulino@warwick.ac.uk; d.bates@warwick.ac.uk).

M. Foo is with the School of Mechanical, Aerospace and Automotive Engineering, Coventry University, CV1 5FB Coventry, U.K. (e-mail: mathias.foo@coventry.ac.uk).

J. Kim is with the Department of Integrative Biosciences and Biotechnology, Pohang University of Science and Technology, Pohang 37673, South Korea (e-mail: jongmin.kim@postech.ac.kr).

Digital Object Identifier 10.1109/LCSYS.2019.2918977

2475-1456 © 2019 IEEE. Personal use is permitted, but republication/redistribution requires IEEE permission.
See http://www.ieee.org/publications_standards/publications/rights/index.html for more information.

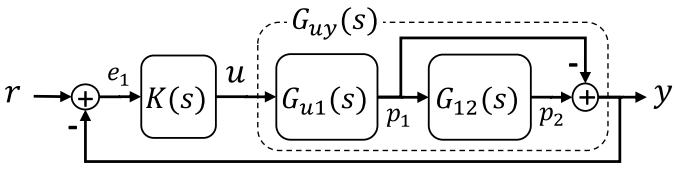

Fig. 1. Linear negative feedback for reference tracking, with a linear plant $G_{uy}(s)$ decomposed into two first order systems $G_{u1}(s)$ and $G_{12}(s)$. A subtraction is necessary to compute the output y from the states p_1 and p_2.

represented by

$$a_1X_1 + a_2X_2 \xrightarrow{\gamma} bX_3$$

where the reactants on the left are converted into the product X_3 on the right at a rate γ, according to the stoichiometric coefficients a_1, a_2 and b. We model the evolution of the concentration x_j of the species X_j with ordinary differential equations (ODEs), derived from mass action kinetics [17]. For the example above, we have

$$\begin{aligned}\dot{x}_1 &= -a_1\gamma x_1^{a_1}x_2^{a_2}\\ \dot{x}_2 &= -a_2\gamma x_1^{a_1}x_2^{a_2}\\ \dot{x}_3 &= b\gamma x_1^{a_1}x_2^{a_2}.\end{aligned} \tag{1}$$

A. Dual Rail Representation and Notation

Consider the negative feedback system in Fig. 1. Since concentrations are non-negative, they are ill suited to represent the subtraction $e_1 = r - y$, where e_1 is a real number. We apply, instead, the *dual rail* representation of [10].

Definition 1: Take two chemical species X^+ and X^-, and their respective non-negative concentrations $x^+(t) \geq 0$ and $x^-(t) \geq 0$. A real signal $x(t) \in \mathbb{R}$ is represented by $x(t) = x^+(t) - x^-(t)$, with dynamics given by $\dot{x}(t) = \dot{x}^+(t) - \dot{x}^-(t)$.

For brevity, time dependency is implicit, i.e., $x \equiv x(t)$, $x^* \equiv x(\infty)$ represents steady state conditions, and $X(s)$ is the Laplace transform of x. We also adopt the notation in [10], [13], where $x^\pm$ represents simultaneously the two concentrations, and $X^\pm$ represents both species. The expression $Y^\pm \xrightarrow{\gamma} Y^\pm + E_1^\mp$ is an abbreviation for the two parallel reactions $Y^+ \xrightarrow{\gamma} Y^+ + E_1^-$ and $Y^- \xrightarrow{\gamma} Y^- + E_1^+$.

Since $x^+ - x^-$ admits infinite combinations for the same value of x, an annihilation reaction $X^+ + X^- \xrightarrow{\eta} \emptyset$ is put in place for each signal, with a very fast reaction rate η [10], [11]. Ideally, the coexistence of the two species X^+ and X^- is eliminated, resulting in either $x \approx x^+$ or $x \approx -x^-$ [10]. Dimensionally, the signal x retains the units of $x^\pm$ (e.g., nM).

The input and output signals of a transfer function $X_j(s) = G_{ij}(s)X_i(s)$ are indicated in the subscripts, and its static gain is written as $G_{ij}(0)$.

B. CRN Representation for a Plant With Delay Approximation

Here we introduce a new method for representing time-delays using the dual rail CRN formulism.

Definition 2: A First Order and Time Delay (FOTD) system, with gain β, a pole at $s = -\alpha^{-1}$, and a phase delay θ, can be expressed in the frequency domain as

$$F(s) = \frac{\beta}{1 + s\alpha}e^{-\theta s} \tag{2}$$

The FOTD plant is commonly used to approximate more complex systems into a simpler form suitable for tuning rules of PID controllers [18], while remaining complex enough to represent bandwidth, gain and phase of a system, which are critical metrics for linear feedback design. In biomolecular systems, the pole can represent the effects of degradation and dilution, while the phase can capture signalling delays.

Definition 3 (Plant): Modelling the delay θ with the first order Padé approximation, the FOTD system in (2) is approximated by the transfer function

$$G_{uy}(s) = \frac{\beta}{1+s\alpha}\frac{2-\theta s}{2+\theta s} = \underbrace{\frac{g_1}{s+g_2}}_{G_{u1}(s)}\left(\overbrace{\underbrace{\frac{g_3}{s+g_4}}_{G_{12}(s)} - 1}^{G_{1y}(s)}\right) \tag{3}$$

where $g_1 = \beta\alpha^{-1}$, $g_2 = \alpha^{-1}$, $g_3 = 4\theta^{-1}$, and $g_4 = 2\theta^{-1}$.

The plant (3) is decomposed into two first order systems, with intermediary states p_1 and p_2, as shown in Fig. 1. The approximation of the delay introduces a non-minimum phase zero at $s = 2\theta^{-1}$.

Result 1: Using the *dual rail* representation, we assign species to each signal according to Section II-A, to arrive at the CRN representation of a plant with a time-delay

$$U^\pm \xrightarrow{g_1} U^\pm + P_1^\pm, \quad P_1^\pm \xrightarrow{g_2} \emptyset, \quad P_1^+ + P_1^- \xrightarrow{\eta} \emptyset \tag{4a}$$
$$P_1^\pm \xrightarrow{g_3} P_1^\pm + P_2^\pm, \quad P_2^\pm \xrightarrow{g_4} \emptyset, \quad P_2^+ + P_2^- \xrightarrow{\eta} \emptyset \tag{4b}$$
$$P_1^\pm \xrightarrow{\gamma} P_1^\pm + \boldsymbol{Y^\mp}, \quad P_2^\pm \xrightarrow{\gamma} P_2^\pm + Y^\pm, \quad Y^\pm \xrightarrow{\gamma} \emptyset \tag{4c}$$
$$U^+ + U^- \xrightarrow{\eta} \emptyset, \quad Y^+ + Y^- \xrightarrow{\eta} \emptyset \tag{4d}$$

Writing the mass action kinetics, the ODEs for (4) are given by

$$\dot{p}_1^\pm = -g_2p_1^\pm + g_1u^\pm - \eta p_1^+p_1^- \tag{5a}$$
$$\dot{p}_2^\pm = -g_4p_2^\pm + g_3p_1^\pm - \eta p_2^+p_2^- \tag{5b}$$
$$\dot{y}^\pm = -\gamma y^\pm + \gamma \boldsymbol{p_1^\mp} + \gamma p_2^\pm - \eta y^+y^-. \tag{5c}$$

C. I/O Dynamics of the CRN Representation

Definition 4: The Input-to-Output (I/O) dynamics of (3) is the response of the CRN dynamics in (5), from the input $u = u^+ - u^-$ to the outputs $p_j = p_j^+ - p_j^-$ and $y = y^+ - y^-$, [10].

The dynamics for $\dot{p}_j = \dot{p}_j^+ - \dot{p}_j^-$ and $\dot{y} = \dot{y}^+ - \dot{y}^-$ are linear because the bimolecular terms cancel out (see details in [10], [19]), and the I/O dynamics do not depend on η. Although we recover $G_{u1}(s)$ from (5a) and $G_{12}(s)$ from (5b), the I/O dynamics are an approximation of $G_{uy}(s)$ in (3). Due to the representation of subtraction, the additional dynamics

TABLE I
PARAMETRISATION FOR THE CRN REPRESENTATION OF THE PLANT

Parameter	Value	Units	Rates	Value	Units
θ	10^5	s	g_1	5×10^{-6}	s^{-1}
α	2×10^5	s	g_2	5×10^{-6}	s^{-1}
β	1	-	g_3	4×10^{-5}	s^{-1}
			g_4	2×10^{-5}	s^{-1}
			γ	2.5×10^{-4}	s^{-1}

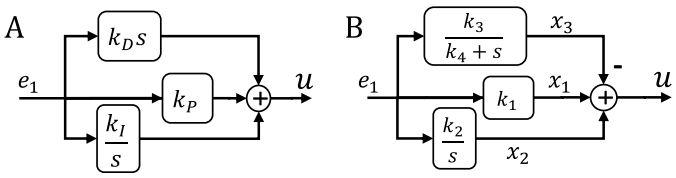

Fig. 2. A) Architecture of a *PID* controller. B) Architecture for $K(s)$ in (9) using the approximation of the derivative $\mathcal{D}(s)$ in (8).

in (5c) with crossed contributions P_1^+ to Y^- and P_1^- to Y^+, result in an exact subtraction only at steady state

$$0 = -\gamma y^{\pm *} + \gamma p_1^{\mp *} + \gamma p_2^{\pm *} - \eta y^{+*} y^{-*}$$
$$\Rightarrow y^* = y^{+*} - y^{-*} = p_2^{+*} - p_2^{-*} - p_1^{+*} + p_1^{-*} = p_2^* - p_1^*$$

The parameterisation of the plant and the resulting reaction rates in the CRN are provided in Table I. The bimolecular reactions in [4] are limited by the maximum feasible hybridisation rate and concentrations of DNA strands, and the timescale and rates of the plant were set accordingly, for a realistic and feasible parameterisation suitable for direct translation into DSD reactions.

III. CRN Representation of PID and State Feedback Controllers

We now introduce new CRN representations of two important classes of reference tracking controllers.

A. Proportional-Integral-Derivative (PID) Control

Definition 5: Define the classical PID as the control law depicted in Fig. 2A, with the actuation $U(s)$ given by

$$U(s) = \left(k_P + k_I s^{-1} + k_D s\right) E_1(s). \tag{6}$$

1) Approximation of the Derivative: We approximate the limit for the differentiation of a signal v as the difference between the signal without and with a delay of τ seconds $\dot{v}(t) \approx \tau^{-1}(v(t) - v(t-\tau))$. Replacing the delay with its Padé approximation results in a transfer function with zero relative degree

$$\frac{\left(1 - e^{-\tau s}\right)}{\tau} \approx \frac{1}{\tau}\left(1 - \frac{2 - \tau s}{2 + \tau s}\right) = \frac{2s}{2 + \tau s}. \tag{7}$$

Definition 6: The transfer function of zero relative degree

$$\mathcal{D}(s) := \frac{2s}{2 + \tau s} = \frac{2}{\tau} - \frac{4}{2\tau + \tau^2 s} \approx s, \ |s| \ll \frac{2}{\tau} \tag{8}$$

closely approximates the derivative over a frequency domain satisfying $|s| \ll 2\tau^{-1}$.

Remark 1: The frequency domain where the approximation (8) is valid depends on a single parameter τ, where a smaller τ results in a larger bandwidth (Fig. 3). Its parameterisation can be naturally related with the frequency description of the plant and specifications of the controller.

Definition 7: Define the modified PID control law in Fig. 2B, which uses (8) instead of differentiation, to arrive at

$$K(s) = k_P + \frac{k_I}{s} + k_D \frac{2s}{2 + \tau s} = k_1 + \frac{k_2}{s} - \frac{k_3}{k_4 + s} \tag{9}$$

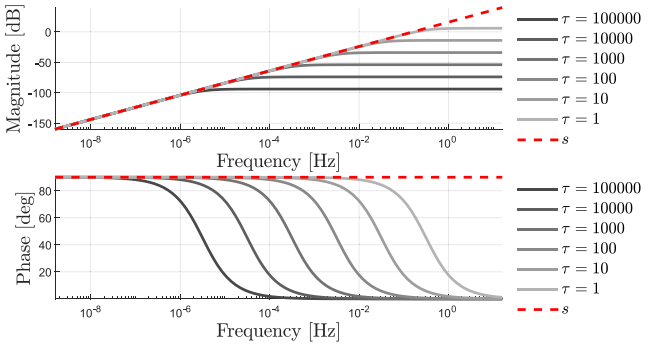

Fig. 3. Comparison of the Bode plots for the derivative s, and the approximation in (8) as function of the delay τ.

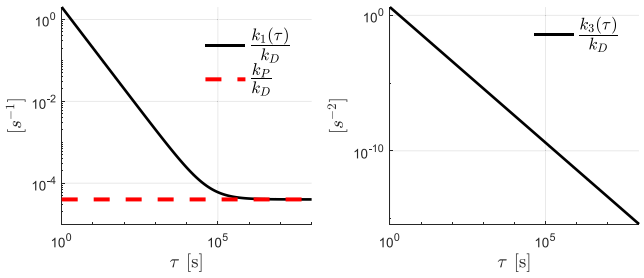

Fig. 4. Dependency of the parameters k_1 and k_3 on the delay τ, used in the control law $K(s)$ in (9).

where $k_2 = k_I$, $k_1 = k_P + \frac{2k_D}{\tau}$, $k_3 = \frac{4k_D}{\tau^2}$, and $k_4 = \frac{2}{\tau}$.

While k_2 depends only on the integral gain k_I, the remaining parameters k_1, k_3 and k_4 depend also on τ. A smaller τ results in a wider bandwidth and a faster pole $s = -k_4$. A larger τ can also be beneficial to filter peaks introduced by the derivative, acting as low pass filter on the delayed signal (similar to the filtered PID controller [18]). However, both k_1 and k_3 depend on the inverse of τ, and quickly increase for a very small delay τ (Fig. 4).

Remark 2: We then have that the physical limits of the reaction rates lead to a tradeoff between having a τ that is large enough for feasible reaction rates, and a τ that is small enough to ensure the bandwidth and accuracy of $\mathcal{D}(s)$.

Remark 3: With the CRNs for the dual rail representation of subtraction, we can represent the transfer function with a zero relative degree (7) as the difference between a static and a dynamic system [18]. This avoids the need for approximations based on *strictly* proper transfer functions, and removes assumptions on saturated regimes or constraints in the parameterisation to disregard higher-order terms (as in [20], [21]).

2) CRN Representation of PID Controller: A CRN is derived, following the formalism of [10] and Section II-A, where species $X_j^{\pm}$ are assigned to each signal x_j in Fig. 2B.

Result 2: The PID control of (9) is represented by

$$R^{\pm} \xrightarrow{\gamma} R^{\pm} + E_1^{\pm}, \quad Y^{\pm} \xrightarrow{\gamma} Y^{\pm} + \boldsymbol{E_1^{\mp}}, \ E_1^{\pm} \xrightarrow{\gamma} \emptyset \tag{10a}$$
$$R^+ + R^- \xrightarrow{\eta} \emptyset, \quad Y^+ + Y^- \xrightarrow{\eta} \emptyset, \ E_1^+ + E_1^- \xrightarrow{\eta} \emptyset \tag{10b}$$
$$E_1^{\pm} \xrightarrow{\gamma k_1} E_1^{\pm} + X_1^{\pm}, \quad X_1^{\pm} \xrightarrow{\gamma} \emptyset, \ X_1^+ + X_1^- \xrightarrow{\eta} \emptyset \tag{10c}$$
$$E_1^{\pm} \xrightarrow{k_2} X_2^{\pm}, \quad X_2^+ + X_2^- \xrightarrow{\eta} \emptyset \tag{10d}$$
$$E_1^{\pm} \xrightarrow{k_3} E_1^{\pm} + X_3^{\pm}, \quad X_3^{\pm} \xrightarrow{k_4} \emptyset, \ X_3^+ + X_3^- \xrightarrow{\eta} \emptyset \tag{10e}$$

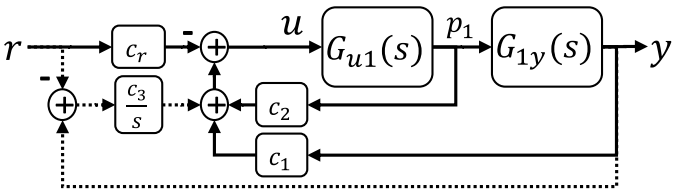

Fig. 5. Structure of static state feedback (gains c_1 and c_2) and feedforward gain control (c_r), extended with integral control $c_3 s^{-1}$ (dashed).

$$X_1^{\pm} \xrightarrow{\gamma} X_1^{\pm} + U^{\pm}, \quad X_2^{\pm} \xrightarrow{\gamma} X_2^{\pm} + U^{\pm}, \; U^{\pm} \xrightarrow{\gamma} \emptyset \tag{10f}$$

$$X_3^{\pm} \xrightarrow{\gamma} X_3^{\pm} + \boldsymbol{U^{\mp}}, \quad U^{+} + U^{-} \xrightarrow{\eta} \emptyset \tag{10g}$$

The error $e_1 = r - y$ is represented in (10a)-(10b), using a CRN similar to (4c). From previous applications to PI controllers [10], [11], we have the CRNs for the gain $x_1 = k_1 e_1$ (10c) and integration $\dot{x}_2 = k_2 e_1$, (10d), and we add the first order system $\dot{x}_3 = -k_4 x_3 + k_3 e_1$ in (10e). The summing junction results from (10f)-(10g), where the crossed contributions to represent the subtraction are highlighted in bold in (10g).

Remark 4: In the case of negative gains, the constraint of positive reaction rates $k_i > 0$, $(i = 1, \ldots, 4)$ can be fulfilled by applying the negative signs in the computation of u. For example, if $k_I < 0$, we keep $k_2 = |k_I| > 0$ and reverse the contributions in (10f) with $X_2^{\pm} \xrightarrow{\gamma} X_2^{\pm} + \boldsymbol{U^{\mp}}$.

B. State Feedback With Integral Control (SFI)

Since we are not dealing with compartmentalised systems, the plant species are in the same solution as the controller species. We exploit the dual rail representation to show for the first time how to design linear state feedback biomolecular controllers, where measurements upstream of the output are used for damping purposes, as an alternative to the derivative gain in PID control.

Definition 8: For the plant in Fig. 1, we have that the error is

$$\mathbf{e} = \begin{bmatrix} e_1 \\ e_2 \\ e_3 \end{bmatrix} = \begin{bmatrix} r - y \\ G_{1y}^{-1}(0) r - p_1 \\ \int e_1 \end{bmatrix} \tag{11}$$

where e_1 is the output tracking error. The second component e_2 is the error between the state p_1 and its steady state condition p_1^*, when $r = y^* = G_{1y}(0) p_1^*$. For the purposes of integral control, we augment the state vector with the integral $e_3 = \int e_1 dt = \int (r - y) dt$.

1) Regulation Problem for Controller Design: For the error defined in (11), we have that $\mathbf{e}^* = 0 \Rightarrow y^* = r$. Hence, we restate the control problem as a regulation problem of the error vector $\mathbf{e}$, considering a static disturbance r. With $\dot{r} = 0$ the error dynamics are $\dot{e}_1 = -\dot{y}$ and $\dot{e}_2 = -\dot{p}_1$, and

$$E(s) = \begin{bmatrix} -G_{uy}(s) \\ -G_{u1}(s) \\ \frac{1}{s}\left(-G_{uy}(s)\right) \end{bmatrix} U(s) \tag{12}$$

The scalars $c_i \in \mathbb{R}$ are solved for the static feedback law

$$U(s) = -\begin{bmatrix} c_1 & c_2 & c_3 \end{bmatrix} E(s) \tag{13}$$

where the closed loop dynamics (12)-(13) have zero steady state error $\mathbf{e}^* = 0$.

2) Controller Structure: Once the gains c_i are set for the problem (12)-(13), we can use (11) to express the actuation u as a functions of p_1, y, and r, and we recover the reference tracking control structure of Fig. 5.

Definition 9: From (11), we have that $c_r = c_2 G_{1y}^{-1}(0) + c_1$, and the static reference tracking control law is written as

$$u = c_1 y + c_2 p_1 - c_3 \int (r - y) - c_r r. \tag{14}$$

Remark 5: Recalling from (3) and Fig. 5 that

$$G_{uy}(s) P_1(s) = G_{u1}(s) G_{1y}(s) P_1(s) = G_{u1}(s) Y(s)$$

we can take (14) and solve for $Y(s) = G_{uy}(s) U(s)$ to obtain the closed loop transfer function as

$$Y(s) = \frac{-G_{uy}(s)\left(c_r + c_3 s^{-1}\right)}{1 - G_{uy}(s)\left(c_1 + c_3 s^{-1}\right) - c_2 G_{u1}(s)} R(s) \tag{15}$$

We then confirm that with integral control we achieve steady state reference tracking, since it follows that

$$\lim_{s \to 0} \frac{Y(s)}{R(s)} = \frac{G_{uy}(s) \frac{c_3}{s}}{G_{uy}(s) \frac{c_3}{s}} = 1. \tag{16}$$

3) CRN Representation: The CRN for the state feedback control law (14) is then given as follows.

Result 3: Assuming negative gains $c_i < 0$ $(i = 1, 2, 3)$ (hence $c_r < 0$), the state feedback in (14) is represented by

$$Y^{\pm} \xrightarrow{\gamma |c_1|} Y^{\pm} + \boldsymbol{U^{\mp}}, \quad P_1^{\pm} \xrightarrow{\gamma |c_2|} P_1^{\pm} + \boldsymbol{U^{\mp}}, \tag{17a}$$

$$R^{\pm} \xrightarrow{\gamma |c_r|} R^{\pm} + U^{\pm}, \quad U^{\pm} \xrightarrow{\gamma} \emptyset, \quad R^{+} + R^{-} \xrightarrow{\eta} \emptyset \tag{17b}$$

$$R^{\pm} \xrightarrow{|c_3|} R^{\pm} + X_0^{\pm}, \quad Y^{\pm} \xrightarrow{|c_3|} Y^{\pm} + \boldsymbol{X_0^{\mp}} \tag{17c}$$

$$X_0^{\pm} \xrightarrow{\gamma} X_0^{\pm} + U^{\pm}, \quad X_0^{+} + X_0^{-} \xrightarrow{\eta} \emptyset \tag{17d}$$

We ensure positive reaction rates in the CRN, by setting them as the absolute values of the controller gains, and addressing the sign of the gains in the catalysis reactions in the summing junctions.

The annihilation reactions for $Y^{\pm}$, $U^{\pm}$ and $P_1^{\pm}$ are included in the CRN of the plant in (4a) and (4d). Both (17a)-(17b) apply the feedback and feedforward gains at steady state, where γ should be on a faster timescale. The reactions (17a) apply the subtractions in (14) by inverting the contributions to U (in bold). The negativity of c_r cancels the minus sign in (14) and results in the catalysis in (17b). The gain and integral of the tracking error are applied in (17c)-(17d).

Remark 6: Comparing (17) to the CRN for the PID controller (10), the state feedback scheme needs fewer reactions and fewer additional species, making it highly attractive for the experimental implementation of feedback with DSD reactions. The CRN simplifies even further without integral control, since removing $X_0^{\pm}$ and (17c)-(17d) reduces the controller to a summing junction. However, this results in a non-zero steady state error.

For example, from Table I we have that $G_{uy}(0) = G_{u1}(0) = G_{1y}(0) = 1$, hence with $c_3 = 0$ we get

$$y^* = -(1 - c_1 - c_2)^{-1}(c_1 + c_2) r \tag{18}$$

The steady state error can be reduced with the use of high gain feedback, but not entirely eliminated.

IV. CRN Dynamics for the Closed Loop Systems

The full dynamics of the CRNs representing each of the closed-loop systems are derived from the mass action law (1). The crossed contributions resulting from the dual representation of the subtractions are highlighted in bold.

For the PID controlller $K(s)$ from (9), we combine the CRNs of the plant (4) and the controller (10). The dynamics are given by the dynamics of the plant (5) together with

$$\dot{e}_1^{\pm} = -\gamma e_1^{\pm} + \gamma \boldsymbol{y}^{\mp} + \gamma r^{\pm} - \eta e_1^{+} e_1^{-} \tag{19a}$$
$$\dot{x}_1^{\pm} = -\gamma x_1^{\pm} + \gamma k_1 e_1^{\pm} - \eta x_1^{+} x_1^{-} \tag{19b}$$
$$\dot{x}_2^{\pm} = k_2 e_1^{\pm} - \eta x_2^{+} x_2^{-} \tag{19c}$$
$$\dot{x}_3^{\pm} = -k_4 x_3^{\pm} + k_3 e_1^{\pm} - \eta x_3^{+} x_3^{-} \tag{19d}$$
$$\dot{u}^{\pm} = -\gamma u^{\pm} + \gamma x_1^{\pm} + \gamma x_2^{\pm} + \gamma \boldsymbol{x_3^{\mp}} - \eta u^{+} u^{-} \tag{19e}$$

For the state feedback controller in (14), combining the CRN of the plant (4) with the CRN from (17), we get the dynamics of the plant (5) together with

$$\dot{x}_0^{\pm} = |c_3| \boldsymbol{y}^{\mp} + |c_3| r^{\pm} - \eta x_0^{+} x_0^{-} \tag{20a}$$
$$\dot{u}^{\pm} = -\gamma u^{\pm} - \eta u^{+} u^{-} + \gamma x_0^{\pm} + \gamma |c_2| \boldsymbol{p_1^{\mp}} + \gamma |c_1| \boldsymbol{y}^{\mp} + \gamma |c_r| r^{\pm} \tag{20b}$$

Similarly to Definition 4, the I/O dynamics of the closed loop systems are given by the response from $r = r^{+} - r^{-}$ to the output $y = y^{+} - y^{-}$ and actuation $u = u^{+} - u^{-}$.

V. Closed-Loop Performance of the Controllers

The controllers are designed for steady state reference tracking, with reduced response times while avoiding tracking overshoot. The controller $K(s)$ in (9) was tuned with the PID block from the MATLAB/Simulink. The response with state feedback was shaped by placing the closed loop poles of (12)-(13) at $(-2 \pm j0.4) \times 10^{-5}$ and -1.6×10^{-6} rad/s, resulting in the parameters in Table II.

The ODE's of the CRNs were simulated in MATLAB/Simulink® to compare the closed-loop transfer functions with the I/O dynamics of the CRNs in Section IV. The response of the FOTD plant $F(s)$ from (2) is compared in Fig. 6A with the approximation of the plant delay from (3), where the output of $G_{uy}(s)$ shows the characteristic initial reversed action from non-minimum phase zeros.

The FOTD system $F(s)$ controlled with the classical PID from (6) is compared in Fig. 6B to the control of $G_{uy}(s)$ using $K(s)$ from (9). The main difference is the non-minimum phase response due to the delay model. The trajectories of the I/O dynamics are different from the closed loop response with $K(s)$, due to the additional dynamics introduced by the subtractions and sums in (19a) and (19e).

Fig. 6C shows the closed loop response with the state feedback control from (14). The controller provides reference tracking with zero steady-state error, for both the transfer function (15) and the I/O dynamics of the CRNs (5) and (20). The non-minimum phase behaviour is introduced by the approximation of the plant delay in (3).

TABLE II
Parametrisation of the Controllers and CRNs

Controller parameters	Parameters for I/O dynamics
$k_P = 2$	$k_1 = 4$
$k_I = 9.5 \times 10^{-6}$ s^{-1}	$k_2 = 9.5 \times 10^{-6}$ s^{-1}
$k_D = 5 \times 10^{5}$ s	$k_3 = 8 \times 10^{-5}$ s^{-1}
$\tau = 5 \times 10^{5}$ s	$k_4 = 4 \times 10^{-5}$ s^{-1}
$c_1 = -0.4064$	$\lvert c_1 \rvert = 0.4064$ s^{-1}
$c_2 = -3.7264$	$\lvert c_2 \rvert = 3.7264$
$c_3 = -6.656 \times 10^{-6}$ s^{-1}	$\lvert c_3 \rvert = 6.656 \times 10^{-6}$ s^{-1}
$c_r = -4.1328$	$\lvert c_r \rvert = 4.1328$
	$\gamma = 2.5 \times 10^{-4}$ s^{-1}

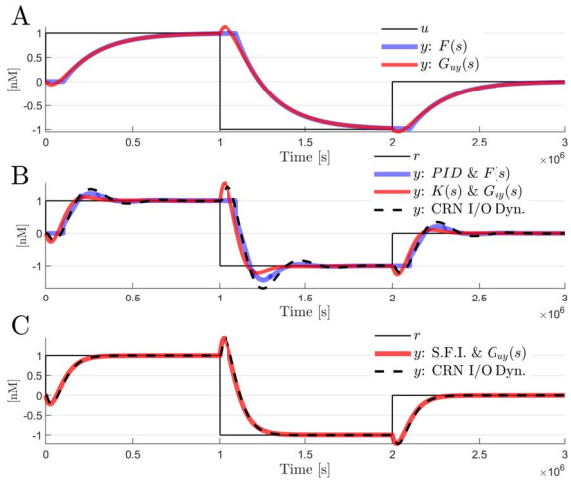

Fig. 6. A) step responses of the FOTD $F(s)$ and the transfer function $G_{uy}(s)$. B) reference tracking with PID control of $F(s)$, with the controller $K(s)$ and $G_{uy}(s)$, and the I/O dynamics from (5) and (19). C) reference tracking with the SFI control, and the I/O dynamics of (5) and (20).

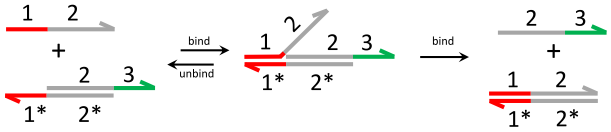

Fig. 7. DSD reaction involving single and double strands with overhanging toeholds. The hybridisation of the toehold 1 to a complementary toehold 1* starts branch migration, displacing the domain 2, releasing the output strands. The strand displacement is irreversible, and the output strand can participate in other reactions, enabling a cascade of multiple reactions.

VI. Verification With DSD Reaction Networks

Fig. 7 illustrates a DSD reaction, where the single-stranded overhangs, termed toeholds, provide initial binding sites for incoming strands to initiate toehold-mediated branch migration, which can result in complete displacement of a strand from its complementary strand, [5], [6]. The work in [4] supplies a framework to translate the three types of reactions used in the CRNs (catalysis, degradation and annihilation) into bimolecular DSD reactions. For example, the unimolecular catalysis reaction $U^{+} \xrightarrow{g_1} U^{+} + P_1^{+}$ is translated into

$$U^{+} + G^{+} \xrightarrow{q_1} O^{+}, \quad O^{+} + T^{+} \xrightarrow{q_{max}} U^{+} + P_1^{+} \tag{21}$$

The *fuel* species G^{+} and T^{+} are consumed irreversibly, and initialised at high concentrations $G^{+}(0) = T^{+}(0) = C_{max}$ (nM),

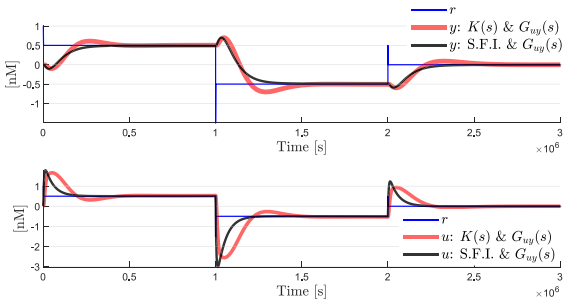

Fig. 8. Deterministic simulations with VisualDSD: time histories of the closed loop output $y = y^+ - y^-$ and the control signal $u = u^+ - u^-$.

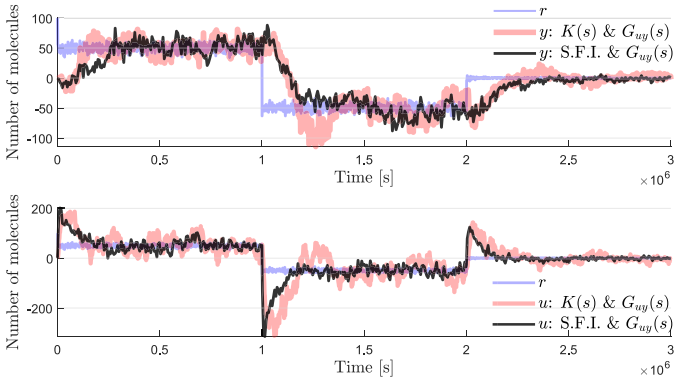

Fig. 9. Stochastic simulation in VisualDSD: time histories of the difference in number of molecules between Y^+ and Y^-, and between U^+ and U^-.

to prevent their consumption from significantly impacting the dynamics. The rate q_{max} $(\text{nMs})^{-1}$ is the maximum strand displacement rate for full toehold binding, and the *bimolecular* reaction rate q_1 is computed from the *unimolecular* rate g_1 with $q_1 = 2g_1/C_{max}$ $(\text{nMs})^{-1}$, assuming the concentrations of the fuel species remain close to C_{max} (further details in [4], [10]).

A. Simulations of DSD Reactions

We validate the experimental feasibility of our designs for implementation with DSD reactions, by demonstrating their correct functioning with the dedicated simulation package VisualDSD [16]. We consider a 2-domain programming structure [5], [11], with feasible values of $C_{max} = 10^4$ nM and $q_{max} = 10^{-3}(\text{nMs})^{-1}$ (from [6]). The conversion of the CRNs with VisualDSD resulted in 128 strands for the PID feedback system, and in 88 strands with state feedback. The time histories of the concentrations with deterministic simulations in Fig. 8, and stochastic simulations in Fig. 9, show successful steady state tracking of the reference signal, and an agreement with the transfer functions of the CRN I/O dynamics.

VII. Conclusions

We have proposed novel CRN representations for plants with time-delays and for two important classes of linear feedback controllers - PID and state feedback. The structure of the PID controller results in a filtered approximation of the derivative, with a fundamental tradeoff in the parameterisation between the accuracy of differentiation and the feasibility of chemical reaction binding rates. The state feedback takes advantage of the ready access of the controller to the chemical species, and it is posed as a regulation problem with zero steady-states. It results in a simpler CRN and requires fewer DNA strand species since it relies mostly on summing junctions. Implementations using DSD reaction networks were successfully verified in VisualDSD, with deterministic and stochastic simulations showing excellent tracking performance.

References

[1] J. Hemphill and A. Deiters, "DNA computation in mammalian cells: MicroRNA logic operations," *J. Amer. Chem. Soc.*, vol. 135, no. 28, pp. 10512–10518, 2013.
[2] B. Groves *et al.*, "Computing in mammalian cells with nucleic acid strand exchange," *Nat. Nanotechnol.*, vol. 11, no. 3, pp. 287–294, 2016.
[3] G. Chatterjee, Y.-J. Chen, and G. Seelig, "Nucleic acid strand displacement with synthetic mRNA inputs in living mammalian cells," *ACS Synth. Biol.*, vol. 7, no. 12, pp. 2737–2741, 2018.
[4] D. Soloveichik, G. Seelig, and E. Winfree, "DNA as a universal substrate for chemical kinetics," *Proc. Nat. Acad. Sci. USA*, vol. 107, no. 12, pp. 5393–5398, 2010.
[5] A. Phillips and L. Cardelli, "A programming language for composable DNA circuits," *J. Roy. Soc. Interface*, vol. 6, no. 4, pp. S419–S436, 2009.
[6] J. X. Zhang *et al.*, "Predicting DNA hybridization kinetics from sequence," *Nat. Chem.*, vol. 10, no. 1, pp. 91–98, 2018.
[7] H. J. Buisman, H. M. M. ten Eikelder, P. A. J. Hilbers, and A. M. L. Liekens, "Computing algebraic functions with biochemical reaction networks," *Artif. Life*, vol. 15, no. 1, pp. 5–19, 2008.
[8] C. Briat, C. Zechner, and M. Khammash, "Design of a synthetic integral feedback circuit: Dynamic analysis and DNA implementation," *ACS Synth. Biol.*, vol. 5, no. 10, pp. 1108–1116, 2016.
[9] R. Brijder, "Computing with chemical reaction networks: A tutorial," *Nat. Comput.*, vol. 18, no. 1, pp. 119–137, 2019.
[10] K. Oishi and E. Klavins, "Biomolecular implementation of linear I/O systems," *IET Syst. Biol.*, vol. 5, no. 4, pp. 252–260, 2011.
[11] B. Yordanov, J. Kim, R. L. Petersen, A. Shudy, V. V. Kulkarni, and A. Phillips, "Computational design of nucleic acid feedback control circuits," *ACS Synth. Biol.*, vol. 3, no. 8, pp. 600–616, 2014.
[12] M. Foo, J. Kim, R. Sawlekar, and D. G. Bates, "Design of an embedded inverse-feedforward biomolecular tracking controller for enzymatic reaction processes," *Comput. Chem. Eng.*, vol. 99, pp. 145-157, Apr. 2017.
[13] T. Y. Chiu, H. J. K. Chiang, R. Y. Huang, J. H. R. Jiang, and F. Fages, "Synthesizing configurable biochemical implementation of linear systems from their transfer function specifications," *PLoS ONE*, vol. 10, no. 9, 2015, Art. no. e0137442.
[14] A. W. K. Harris, J. A. Dolan, C. L. Kelly, J. Anderson, and A. Papachristodoulou, "Designing genetic feedback controllers," *IEEE Trans. Biomed. Circuits Syst.*, vol. 9, no. 4, pp. 475–484, Aug. 2015.
[15] R. Sawlekar, F. Montefusco, V. V. Kulkarni, and D. G. Bates, "Implementing nonlinear feedback controllers using DNA strand displacement reactions," *IEEE Trans. Nanobiosci.*, vol. 15, no. 5, pp. 443–454, Jul. 2016.
[16] M. R. Lakin, R. L. Petersen, and A. Phillips, *Visual DSD User Manual, V0.14 Beta*, Microsoft Res., 2017. [Online]. Available: https://dsd.azurewebsites.net/beta/manual-beta.pdf
[17] P. Tóth and J. Érdi, *Mathematical Models of Chemical Reactions: Theory and Applications of Deterministic and Stochastic Models*. Manchester, U.K.: Manchester Univ. Press, 1989.
[18] K. J. Aström and R. M. Murray, *Feedback Systems: An Introduction for Scientists and Engineers*. Princeton, NJ, USA: Princeton Univ. Press, 2008.
[19] N. M. G. Paulino, M. Foo, J. Kim, and D. G. Bates, "Robustness analysis of a nucleic acid controller for a dynamic biomolecular process using the structured singular value," *J. Process Control*, vol. 78C, pp. 34–44, Jun. 2019.
[20] W. Halter, Z. A. Tuza, and F. Allgöwer, "Signal differentiation with genetic networks," *IFAC-PapersOnLine*, vol. 50, no. 1, pp. 10938–10943, 2017.
[21] M. Chevalier, M. Gómez-Schiavon, A. Ng, and H. El-Samad, "Design and analysis of a proportional-integral-derivative controller with biological molecules," *BioRxiv*, 2018. doi: 10.1101/303545.